The Report Committee for Chison Qishan Liu Certifies that this is the approved version of the following report:

Growth Optimization of WSe_2 and its Sulfurization to WS_2

APPROVED BY SUPERVISING COMMITTEE:

Sanjay Banerjee, Supervisor

Deji Akinwande

Growth Optimization of WSe_2 and its Sulfurization to WS_2

by

Chison Qishan Liu

Report

Presented to the Faculty of the Graduate School of

The University of Texas at Austin

in Partial Fulfillment

of the Requirements

for the Degree of

MASTER OF SCIENCE IN ENGINEERING

The University of Texas at Austin

May 2019

Dedication

In memory of my friend Billy.

Abstract

Growth Optimization of WSe_2 and its Sulfurization to WS_2

Chison Qishan Liu, M.S.E.

The University of Texas at Austin, 2019

Supervisor: Sanjay Banerjee

Tungsten diselenide has gained much interest within recent years after it was reported to have both p-type and ambipolar transport properties. And because most other transition metal dichalcogenides exhibit n-type transport properties, tungsten diselenide would help to further realize CMOS technology if one could find a more reliable way to synthesize it in large areas with high quality crystallinity. In this report I will be detailing my work on successfully synthesizing WSe_2, its sulfurization into WS_2, and discussing what I've observed in both the crystal quality and growth mechanisms. My goal is to provide a better understanding of the growth process in hopes of moving forward with improving future growth recipes.

Table of Contents

List of Figures

INTRODUCTION

Interest in studying two-dimensional (2D) materials, or materials comprised of single atomic layers, roughly began with the isolation of graphene in 2004 first demonstrating its remarkable electrical properties [1]. While there has been considerable research and applications of graphene, attempts to make graphene transistors have realized its lack of a band gap makes them unviable for digital devices since there is no way to turn them off. Over time, researchers began to realize that an undiscovered realm of new science was waiting to be tapped into because many compounds, if possibly most, have the potential to possess unique and extraordinary properties when fabricated into a 2D structure. This has led to studying transition metal dichalcogenides (TMDs) – a family of materials with the general formula MX_2 in which the M can be a transition metal and the X can be a chalcogen.

Interest in 2D TMDs rose after discovering some have semiconducting properties and possess direct bandgaps, especially in molybdenum disulfide (MoS_2) after it was demonstrated on exfoliated samples that transistors could be fabricated on MoS_2 acting as the conductive channel [2]. The electrical properties of TMDs would also make them effective in optoelectronic devices. Not only that, TMDs possess many other characteristics such as high-quality interfaces without out-of-plane dangling bonds, mechanical flexibility, and tunable bandgaps. And while MoS_2 is one of the most widely studied, tungsten diselenide (WSe_2) has seen an increased interest within the past few years. This is because MoS_2 exhibits unipolar, n-type transport characteristics while Wse_2 has predominately p-type conduction but can be configured have n-type transport due to its ambipolar capabilities [3]. Coupled with its TMD properties and smaller bandgap, this has led to interest in Wse_2 devices such as digital devices, optoelectronics, valley-based electronics. But most fervently is interest in developing pMOS and ambipolar transistors which would open way for CMOS technology [3].

PURPOSE OF STUDY

The ultimate goal of TMD crystal growth optimization is to cover larger areas with monolayers. The purpose of this study is to work on optimizing the growth recipe of WSe_2 and report on the structure and quality of successful synthesis. In doing so the hope is to get a better understanding of the growth mechanisms at play to improve and guide us in recipe optimization to potentially produce more samples at higher quality. Samples of high-quality WSe_2 structures can be utilized by researchers in device fabrication that have an interest in it. In addition, we'll be looking at the outcome of an additional process to sulfurize WSe_2 into tungsten disulfide (WS_2).

EXPERIMENTAL SECTION

MATERIAL SYNTHESIS PROCESS

Figure 1 depicts a cartoon schematic of the CVD growth system used for the synthesis of WSe_2. The chamber is comprised of a quartz tube with an inner diameter of 22 mm enclosed by a furnace. A heating tape is wrapped around the tube upstream from the edge of the furnace. The precursors used for growth are solid powders of tungsten trioxide (WO_3) (Sigma-Aldrich, CAS: 1314-35-8, 99.995%) and selenide (Sigma-Aldrich, CAS: 7782-49-2, 99.99%). The target substrate is double-side polished 285 nm SiO_2 on moderately doped p-type Si. The background gas during the growth was hydrogen which is flowed upstream and is controlled by a Mass Flow Controller (MFC). The direction of gas flow begins at the MFC and propagation of the background gas and evaporated precursors was controlled by a vacuum pump downstream. The setup begins with loading 15 mg of WO_3 into the alumina crucible at roughly one third of its length. Then the target substrate is placed on top of the crucible and both are loaded into the center of the furnace. Next, a second crucible is loaded with 1.5 g of selenium powder. This crucible is loaded into the quartz tube to where it sits in the middle of the heating tape. Afterwards, the chamber is sealed up and the vacuum pump is opened to start cleaning the entire line of atmospheric gases and to pump the system down to base pressure of ~20 mTorr.

The growth process begins by setting the MFC to flow 160 sccm of hydrogen and tightening the valve of vacuum pump until the chamber pressure reads ~400 Torr. Then the furnace is turned on and set to reach 850°C. Once the furnace has reached a temperature of 550°C the heating tape is turned on and set to reach 270°C. When the furnace reaches 850°C, the temperature is held there for 5 minutes while adjusting the valve of the vacuum pump to ensure that the total pressure of the chamber is continuously throttled at 400 Torr during the growth process. After 5 minutes the furnace is turned off and allowed to cool down to room temperature for removal. The heating tape is turned off once the furnace has dropped back to 550°C.

Afterwards, the samples are characterized and select samples continue to the sulfurization process.

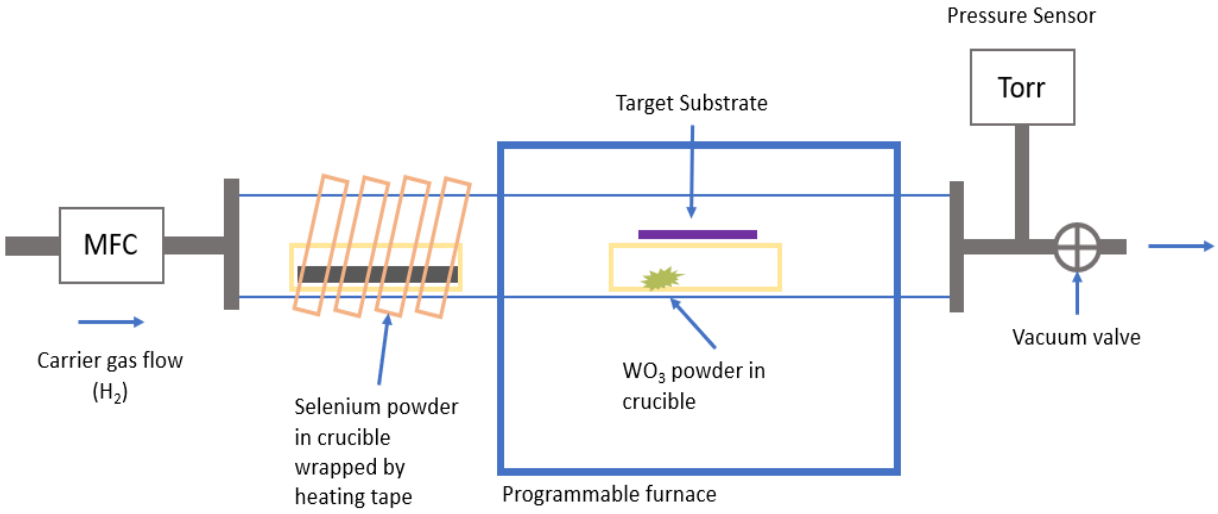

Figure 1: Schematic of CVD growth system for WSe_2.

SULFURIZATION PROCESS

Figure 2 depicts the sulfurization process. A separate CVD system (quartz tube, MFC lines, furnace, and vacuum pump) is utilized in order to avoid cross-contamination of sulfur and selenide between growth systems. The setup begins by placing a sample grown with WSe_2 into the center of the furnace. Then a crucible is loaded with sulfur powder (Sigma-Aldrich, CAS: 7704-34-9, 99.998%) and placed in the center of the heating tape. Afterwards, the system is closed, and vacuum is pulled to begin the pumping process to bring the system down to base pressure (~20 mTorr). This is followed by 2 purge cycles using nitrogen at 200 sccm where it is over pressurized to >900 Torr and then vacuum is pulled to return to base pressure. The purge cycles are to guarantee the removal of atmospheric contamination before sulfurization. Lastly, the pressure is brought above 900 Torr and the atmosphere exhaust is opened.

Sulfurization begins by changing the MFC's to flow 5 sccm of nitrogen and 5 sccm of hydrogen. The gas flow from the MFC's will ensure a constant downstream flow across the CVD

chamber to the exhaust and avoid backflow from the atmospheric gases. The furnace is turned on and set to reach 850°C. Once it reaches 550°C, the heating tape is turned on and set to reach 150°C. Then, after the furnace has reaches 850°C, the temperature is held there for 30 minutes. After 30 minutes both the heating tape and furnace are turned off to allow the chamber to cool down to room temperature. Lastly, the sulfurized sample is taken for final characterization.

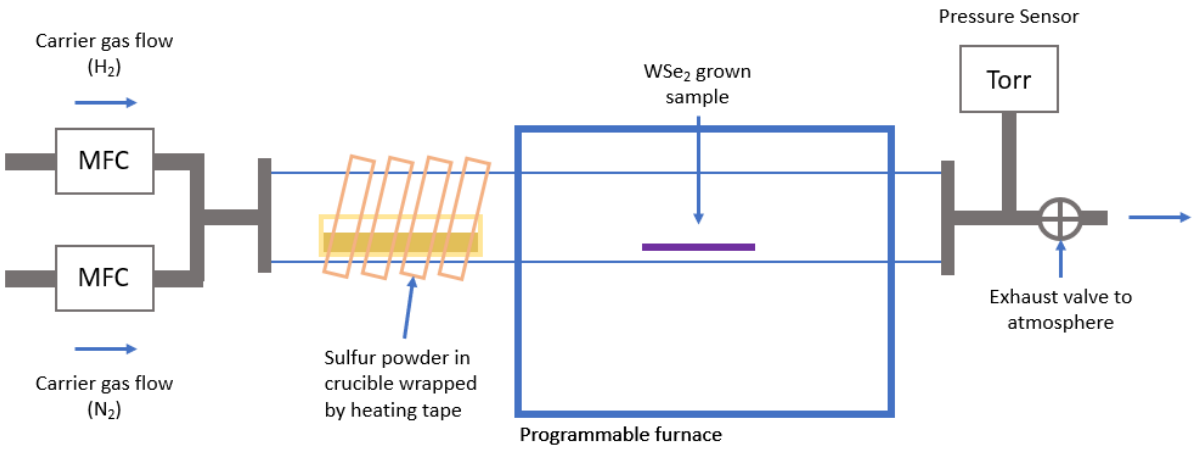

Figure 2: Schematic for sulfurization system.

CHARACTERIZATION

Optical images are taken by optical microscope. Material characterization is performed by Raman and photoluminescence (PL) spectroscopy using Renishaw inVia Raman spectrophotometer system coupled with 532 nm green laser.

RESULTS AND DISCUSSION

AS-GROWN WSE2 DISCUSSION

High quality samples of WSe_2 with usable areas were successfully grown. The most promising samples with WSe_2 are depicted in Figure 3. These samples contain areas of high-quality monolayer crystalline structures and are typically found in a similar pattern as Figures 3a to 3c - islands of WSe_2 where the center is bulk growth that grows perpendicular to the substrate in a fractal pattern and the edges fan out in a monolayer fashion. PL and Raman response of the monolayer regions are plotted in Figures 3d and 3e, respectively. A strong PL response can be seen with a distinct peak at 781 nm. This high-quality of a response would only be present for a monolayer structure. The Raman spectra reports a primary peak at 258 cm^{-1} and a secondary peak is reported at 229 cm^{-1}, annotated by "1" and "2," respectively.

Although most Raman signatures of WSe_2 found in literature describe a primary peak at 250 cm^{-1}, most are measured using exfoliated samples of WSe_2 which is known to alleviate strain [5]. Our as-grown samples form intersected domains which puts more strain on the structures compared to isolated domains. Instead, our Raman spectra matches reported work of strained WSe_2 which would be causing the blue shift, especially if the artifact in Figure 3c annotated as "3" is the emerging separation between the E^1_{2g} and A_{1g} vibrational modes [4]. The effects of strain may also explain why our measured PL response has been shifted to a higher wavelength from 752 nm to 781 nm. In addition to the high-quality PL response, the absence of a Raman signature near 309 cm^{-1} also supports a monolayer structure (see Figure 5e) [5]. The presence of a peak disappears at single layers and is only observed for layers of two or more.

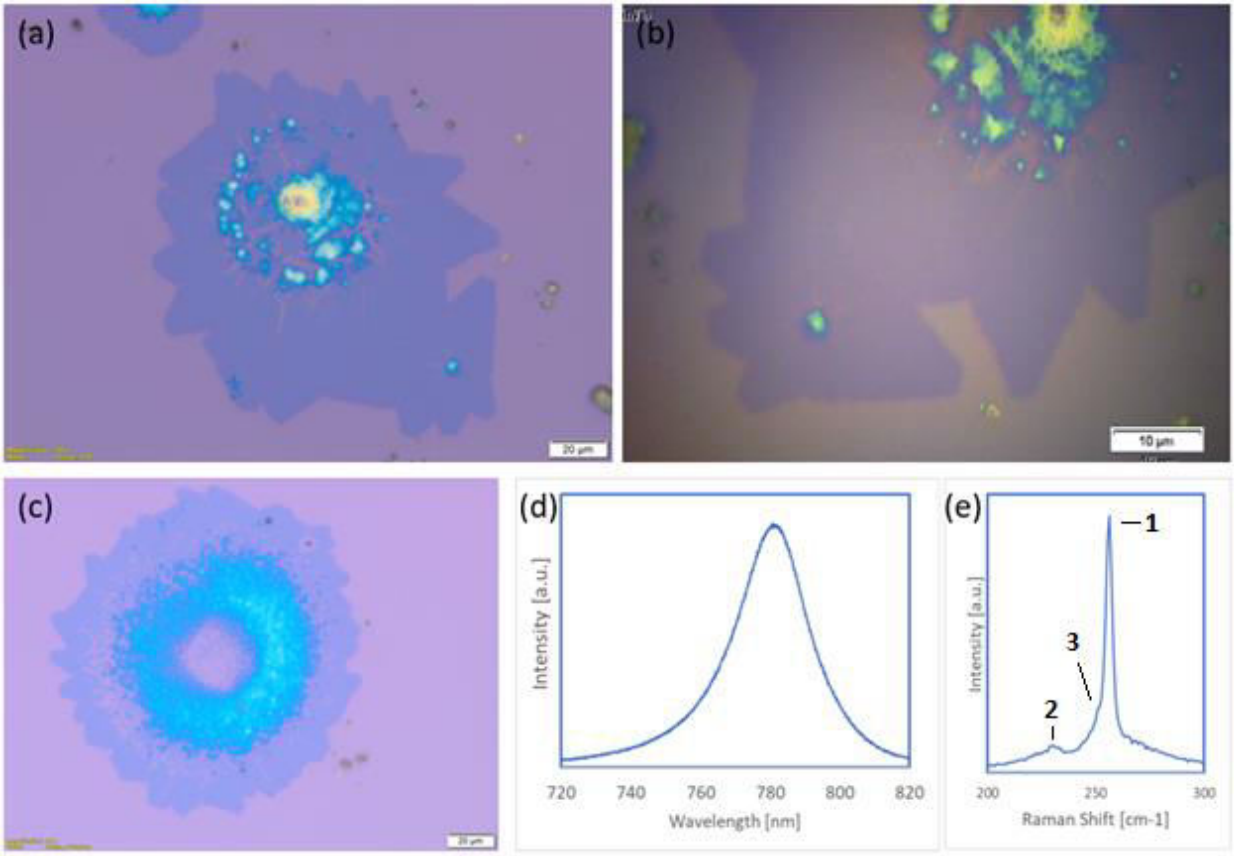

Figure 3: Regions of monolayer domains of Wse_2. a) – c) are optical images depicting islands with a bulk fractal growth center and monolayer edges. d) is the PL response taken at the monolayer regions. E) is the Raman shift taken at the monolayer regions.

Another growth formation observed is depicted in Figure 4. Instead of individual islands with fractal centers, Figure 4a is an optical image which depicts how larger areas of continuous WSe_2 growth transitions from bulk growth (bottom right) into silicon substrate (top left). Two points are measured for their Raman and PL spectras depicted in Figures 4b and 4c, respectively. The line plots in Figures 4b and 4c colored orange (or blue) correspond to the orange (or blue) "X" in Figure 4a as the general location of where the spectras were measured. The motivation is although the orange spot has the same optical contrast seen in Figure 3, the blue spot still appears to have some form of deposition since the Raman signature isn't only silicon oxide. The Raman spectras in Figure 4b both have a primary peak at 252 cm^{-1} and a secondary flattened peak across

the 255 – 265 cm^{-1} range. They both have a signature at 309 cm^{-1} which suggests bilayer or greater. These match more closely to exfoliated Raman samples referenced earlier, although their PL maximum is closer to those of Figure 3 [5]. The inset of Figure 4b compares the intensities of both blue and orange PL responses to that of Figure 3d colored in grey.

Even though the structure indicates a bilayer, Figure 4 illustrates the potential for further optimization of the WSe_2 growth recipe. The objective is to cover more area with less layers and possibly one day have a consistent growth method to cover large areas with a single atomic layer of WSe_2. It can be seen from Figure 4a that at a certain point near the orange it is energetically favorable for the WSe_2 crystal gradient to form single crystals that grow and combine laterally with less vertical propagation.

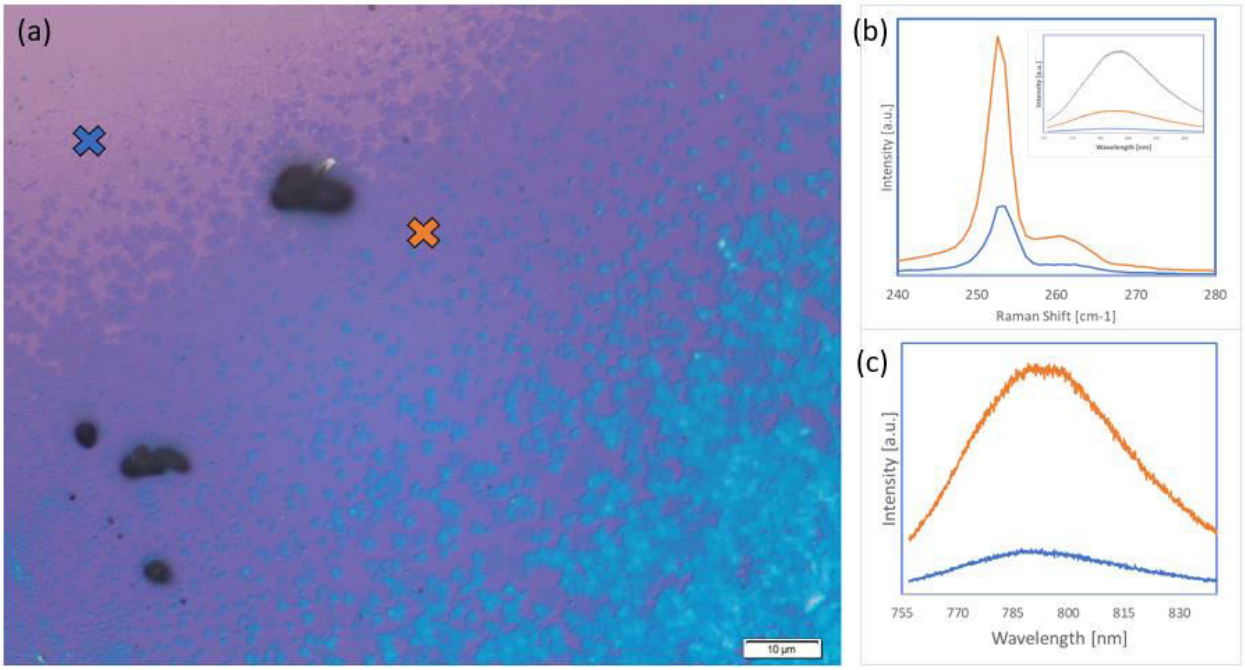

Figure 4: Fanout growth of WSe_2. a) Optical image of Wse_2 growth receding to thinner layers from right to left. b) Raman shift taken at two points (line graph color corresponds to colored "X" in the optical image). c) PL response taken at two points. Inset of b) compares intensities of c) to PL response of Figure 3d.

Growth Mechanism

One observation noted is the total evaporation of the WO_3 precursor. This is done by a rough visual inspection of the crucible that held the substrate and WO_3 by nothing how much of the crucible remains the same color or how much of the crucible surface is coated. Even though all samples reported previously have evidence for high WO_3 evaporation, there may be evidence that suggests different types of nucleation. Crystal domains and other structures that report high crystallinity and PL responses tend to be found branching out of clusters of bulk crystal WSe_2 at their origin (Figures 3a – 3c and Figure 5). These areas also happen to be found more often near clusters of unevaporated deposits of WO_3 on the substrates. The hypothesis is the majority of high-quality structures comes from heterogenous nucleation where WO_3 has deposited onto the substrate.

Figure 5 may support this nucleation theory if it can be assumed that Figures 5a or 5c began formation around a deposit of WO_3 until it was fully evaporated or left and has now formed a well of bulk crystals. Figure 5b may be when a WO_3 deposit didn't fully evaporate given that each optical image is comparable in size. The PL and Raman responses of monolayers (1L) and bilayers (2L) are plotted in Figures 5d and 5e, respectively. The PL intensities have been normalized the 1L maximum and the 2L response is multiplied by 2 to illustrate curvature. The Raman peak difference 1L and 2L is only 1 cm^{-1} so a more recognizable difference is the presence of the bilayer shift at 310 cm^{-1} (Figure 5e). Areas that have 1L, 2L, or greater thicknesses (>2L) are annotated in Figures 5a – 5c.

Samples with any WSe_2 growth, high-quality or not, tend to not have much total deposition compared to other TMD growth recipes such as MoS_2 even if a crucible indicates high evaporation. The sidewall contamination of the quartz tube is noted to be relatively minimal as well. This may be due to the higher evaporating point and heavier weight of the WO_3 leading to less vertical dispersion and hitting the target substrate. In which case, there may be potential to increase the yield of WSe_2 growths with experiments that focus on lateral diffusion of WO_3. One

example would be depositing WO_3 precursor onto substrates in a controlled, variable manner. Or placing the target substrate downstream from where the WO_3 is held, and so on.

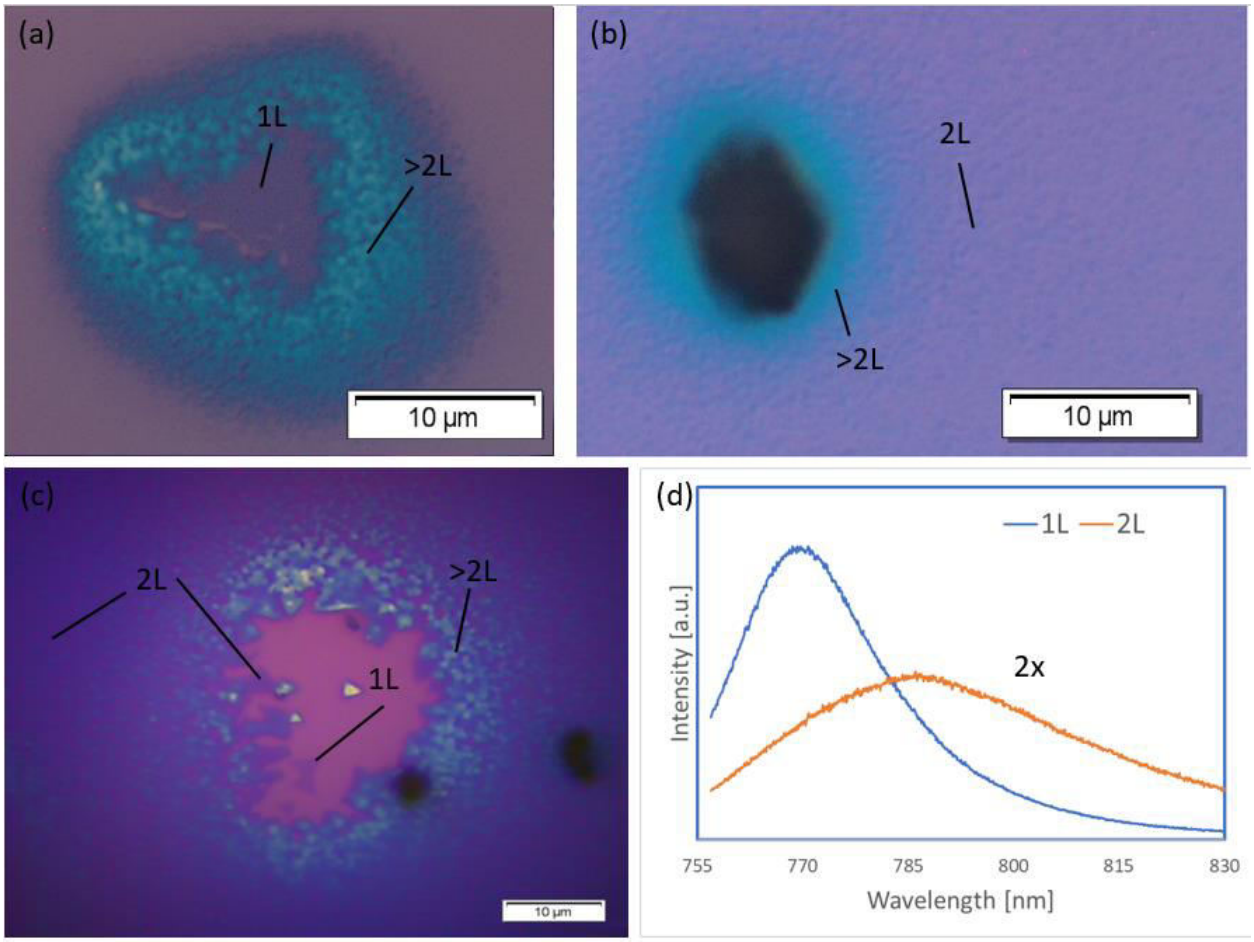

Figure 5: WO_3 evaporations and characterization. a) and c) Optical images of WSe_2 growth where WO_3 nucleation may have started. b) Optical image of WSe_2 growth where WO_3 is found (in black) as the nucleation site. Various locations of 1L, 2L and bulk (>2L) are noted for contrast. d) Normalized Pl response between 1L and 2L.

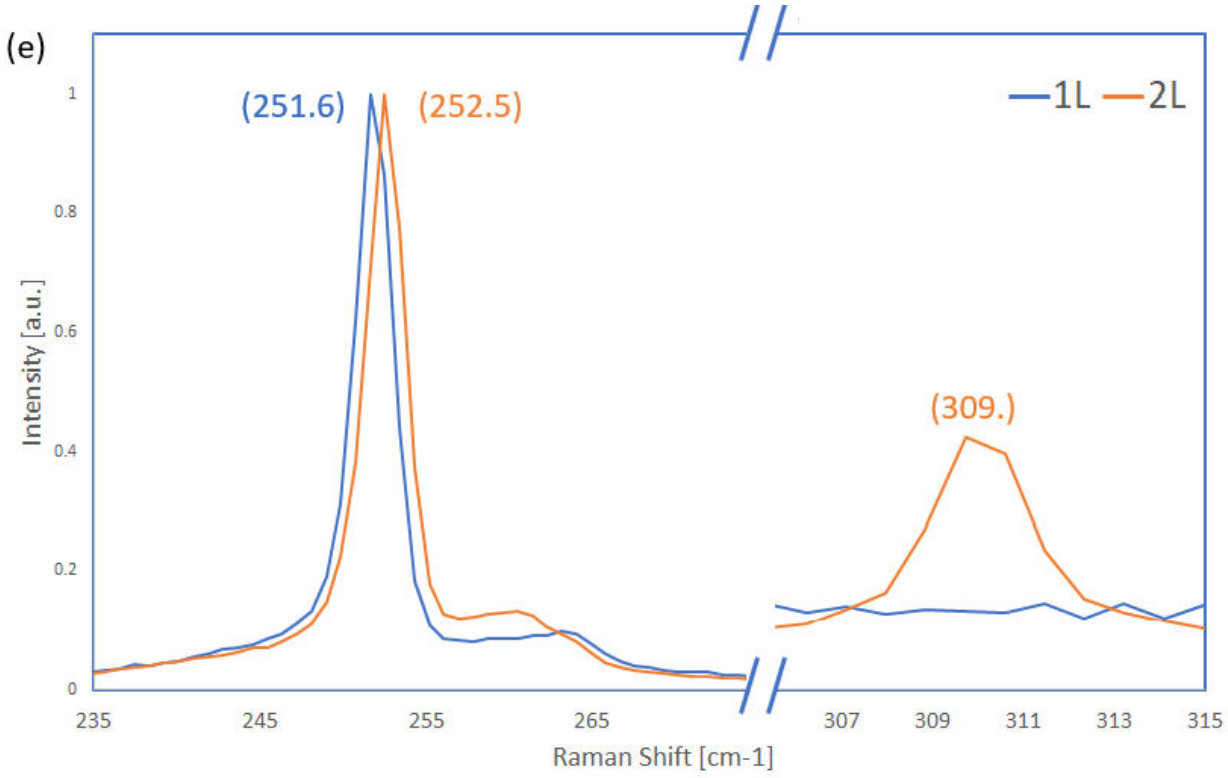

Figure 5, cont.: e) Raman spectras between 1L and 2L.

Crystallinity

Some growths with high deposition were observed to have areas that were less crystalline and more film-like in composition with a coverage of around a few centimeters in area. These areas tend to form directly above where the WO_3 was placed on the crucible but aren't found to be near solid WO_3 deposits. Figure 6 compares the Raman spectra and optical image of the film vs. a WSe_2 domain from Figure 3b. PL response is nonexistent from the film. The optical contrast of Figure 6b is reminiscent of other TMDs grown through metal organic CVD means which may indicate the deposition is more of a film as opposed to a crystalline structure. One theory is the two peaks found at 242 cm^{-1} and 253 cm^{-1} is reminiscent of bulk WSe_2 spectra when both vibrational modes begin to separate, although this is only speculation. Regardless, these samples aren't as usable to device researchers unlike those in Figure 3 and were utilized for our

sulfurization experiments. As well as putting it to use, this helps build our library of spectras to identify for future growth work.

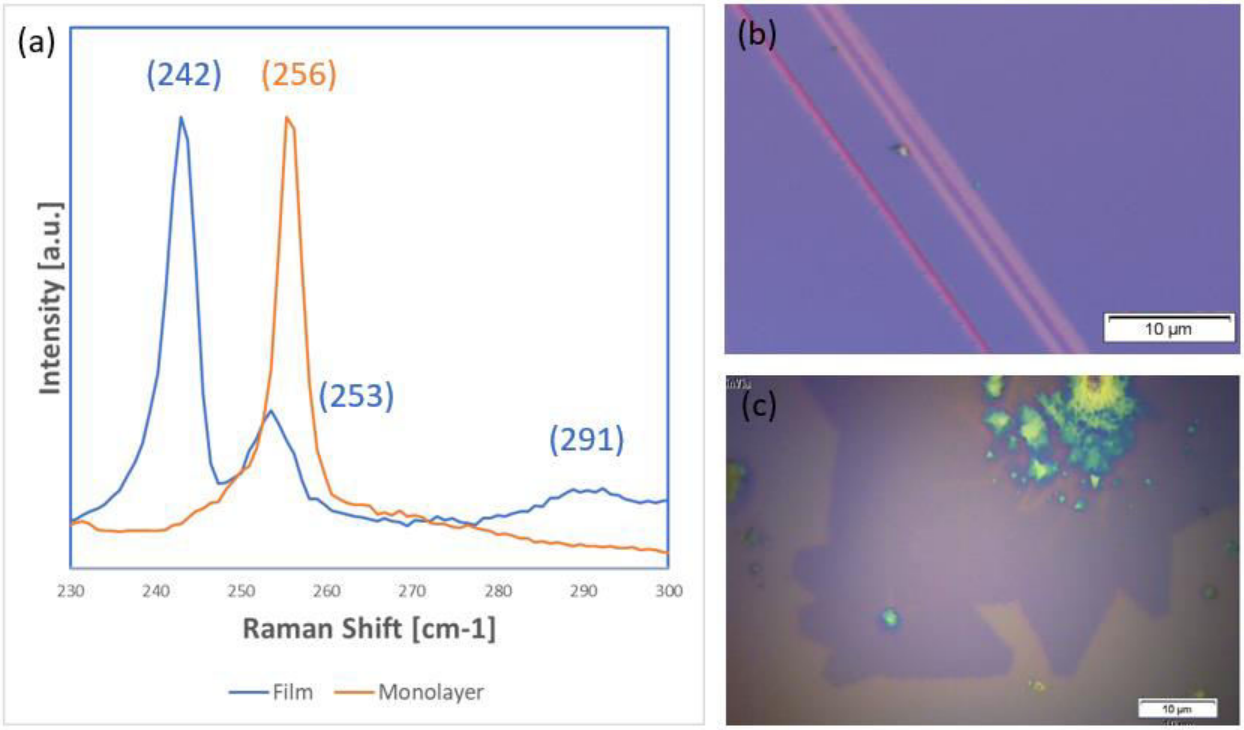

Figure 6. WSe_2 Film vs. domains. a) Compares the Raman spectra of the film vs. domains from Figure 3. b) Optical image of film formation with surface scratch imposed for optical contrast. c) Repeated image of Figure 3b.

SULFURIZED WS_2 DISCUSSION

The criteria for selecting WSe_2 grown samples for sulfurization was to use samples that had high deposition but low crystallinity, i.e. more film-like in appearance as previously discussed. Samples with high crystallinity were used elsewhere. After sulfurization, most areas that were heavily covered experienced negligible optical change and their Raman spectras report that most of the material turned into WS_2 with some ratio of WSe_2 left over. No significant PL was reported in bulk areas. However, Figure 6 details more noteworthy changes. Figure 6a is an

optical image of an as-grown WSe_2 sample downstream (left to right) where the deposition dies off and only the Si/SiO_2 substrate is visible (cyan color vs. pink). Figure 6b is an optical image of the same area where the material has been sulfurized to form triangular structures of WS_2. Figures 6c, 6d, and 6e are Raman and PL spectras between the as-grown WSe_2 (plotted with blue) and annealed WS_2 (plotted with orange). Raman and PL measurements were taken at lower laser intensities after sulfurization to capture a smaller number of structures within a laser spot.

The annealed Raman spectra (Figure 7c) matches WS_2 spectras found in literature with an E^1_{2g} peak at 354 cm^{-1} and an A_{1g} peak at 417 cm^{-1} [6]. The peak-to-peak separation also suggests an average thickness of three to four layers. The absence of a Raman signature from 240 cm^{-1} to 253 cm^{-1} indicates complete selenide-to-sulfur kickout in these structures. A PL response can be seen in Figure 7d with a maximum at 644 nm, within the expected region of WS_2. No PL response was measured from the as-grown sample. Overall, there may be potential in utilizing this phenomenon for future work.

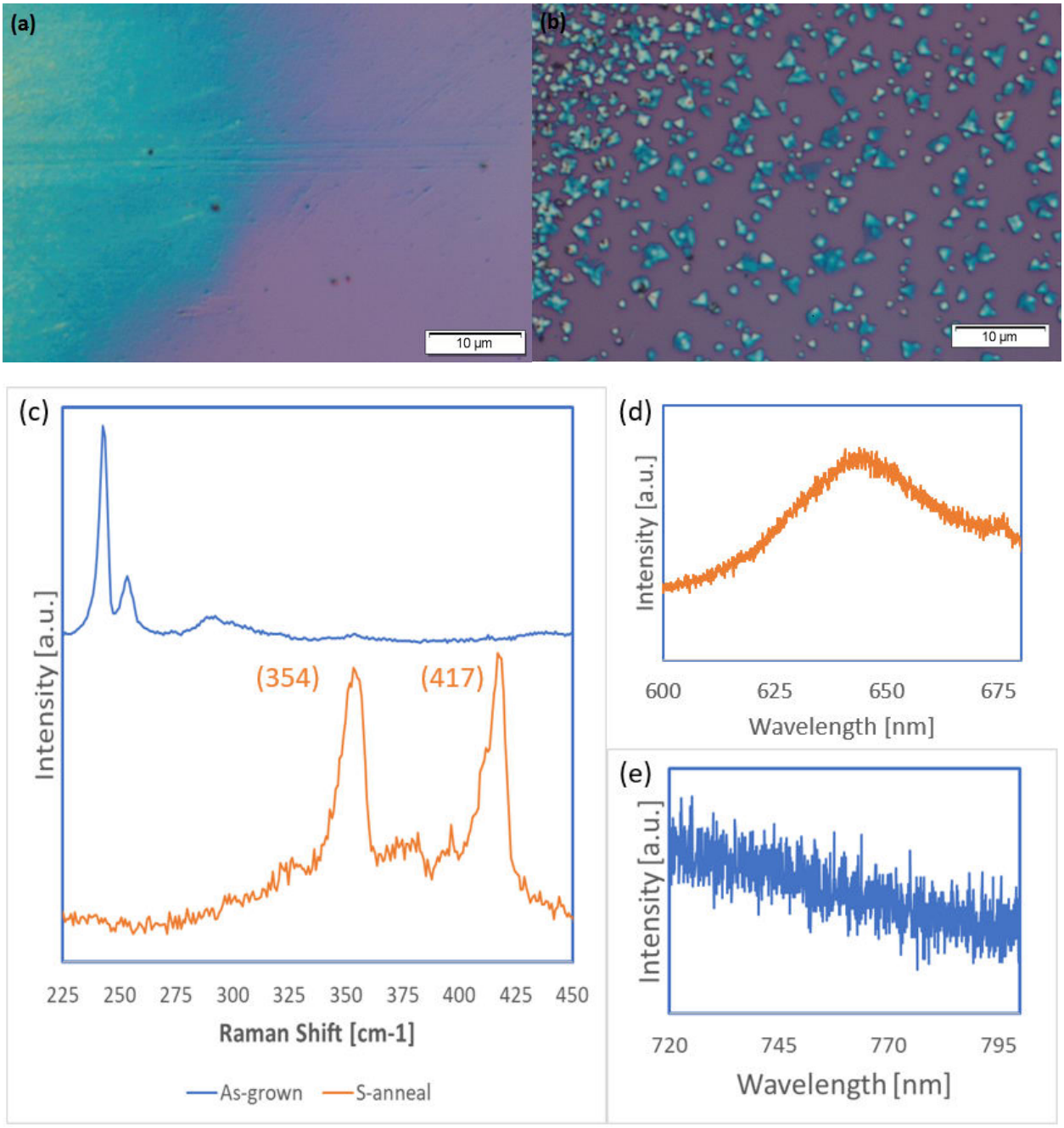

Figure 7. Sulfurization of WSe_2 to WS_2. a) Optical image of WSe_2 film-like deposition in contrast with Si/SiO_2 substrate. b) Optical image of WS_2 crystal structures after sulfurization. c) Raman spectra comparison before and after sulfurization. d) PL response of WS_2 structures. e) PL response of WSe_2 film.

CONCLUSION

In this report, I showed that the synthesis of high quality WSe_2 is possible through CVD of solid precursors. The quality of the structures grown was evaluated and identified through Raman and PL spectroscopy which were matched to previous works of literature. Although the measured Raman and PL response have slight differences, this can be explained by considering the effects of strain on the vibrational modes of TMDs. In addition, there is evidence which highlights that the potential of larger monolayer area growths may be possible through further growth optimization work. Not only would higher coverage be a boon for future research but would also bring us closer to fully realize TMD CMOS integration.

In hopes of moving forward, I've detailed observations about the growth mechanisms of WSe_2 to be largely heterogenous nucleation of the WO_3 and the effects a heavier precursor has on its dispersion compared to MoS_2. This preference may be useful in determining the next steps in growth recipe optimization. As well as taking note of the material's crystallinity variation to build a better library for characterization purposes. Lastly, the sulfurization process has been shown to successfully convert select areas of WSe_2 with low crystallinity into triangular structures of WS_2. Further work to make use of this phenomenon may even be useful in the continuing field of TMD crystal growth.

Bibliography

[1] K. Novoselov, "Electric Field Effect in Atomically Thin Carbon Films", *Science*, vol. 306, no. 5696, pp. 666-669, 2004. Available: 10.1126/science.1102896.

[2] B. Radisavljevic, A. Radenovic, J. Brivio, V. Giacometti and A. Kis, "Single-layer MoS2 transistors", *Nature Nanotechnology*, vol. 6, no. 3, pp. 147-150, 2011. Available: 10.1038/nnano.2010.279.

[3] Z. Wang et al., "The ambipolar transport behavior of WSe2 transistors and its analogue circuits", *NPG Asia Materials*, vol. 10, no. 8, pp. 703-712, 2018. Available: 10.1038/s41427-018-0062-1.

[4] M. Qiao, T. Wang, J. Zhang, Y. Liu, P. Liu and X. Wang, "The effect of carbon-ion irradiation on surface microstructure and photoluminescence properties in monolayer tungsten diselenide", *Nuclear Instruments and Methods in Physics Research Section B: Beam Interactions with Materials and Atoms*, vol. 435, pp. 278-284, 2018. Available: 10.1016/j.nimb.2018.01.003 [Accessed 3 May 2019].

[5] P. Tonndorf et al., "Photoluminescence emission and Raman response of monolayer MoS_2, MoSe_2, and WSe_2", *Optics Express*, vol. 21, no. 4, p. 4908, 2013. Available: 10.1364/oe.21.004908 [Accessed 3 May 2019].

[6] W. Zhao et al., "Lattice dynamics in mono- and few-layer sheets of WS2 and WSe2", *Nanoscale*, vol. 5, no. 20, p. 9677, 2013. Available: 10.1039/c3nr03052k [Accessed 4 May 2019].